Author(s): Rasilo, Paavo & Salem, Aboubakr & Abdallh, Ahmed & De Belie, Frederik & Dupre, Luc & Melkebeek, Jan A.

Title: Effect of Multilevel Inverter Supply on Core Losses in Magnetic Materials and Electrical Machines

Year: 2015

Version: Post print

Please cite the original version:

Rasilo, Paavo & Salem, Aboubakr & Abdallh, Ahmed & De Belie, Frederik & Dupre, Luc & Melkebeek, Jan A. 2015. Effect of Multilevel Inverter Supply on Core Losses in Magnetic Materials and Electrical Machines. IEEE Transactions on Energy Conversion. Volume 30, Issue 2. 736-744. ISSN 0885-8969 (printed). DOI: 10.1109/tec.2014.2372095.

Effect of Multilevel Inverter Supply on Core Losses in Magnetic Materials and Electrical Machines

Paavo Rasilo, Aboubakr Salem, Ahmed Abdallh, Frederik De Belie, Luc Dupré, and Jan A. Melkebeek, *Senior Member, IEEE*

***Abstract*—The effect of multilevel inverter supply on power losses in magnetic cores and electrical machines is studied. A dynamic numerical model for the hysteresis, eddy current, and excess losses in a core lamination is first developed. By both measurements and simulations for a ring-core inductor, we demonstrate how increasing the number of inverter voltage levels decreases the iron losses when compared with traditional two-level supply. Although the switching frequency has a significant impact on the iron losses in the case of a traditional two-level inverter, using three or five voltage levels makes the losses almost independent of the switching. Finally, finite-element simulations show that similar reductions are also possible for the core losses of 150-kVA and 12.5-MW wound-field synchronous machines, in which rather low switching frequencies are typically used. Calorimetric loss measurements are also presented for the 150-kVA machine in order to confirm the significant effect of switching frequency on the core losses with two-level inverter supply.**

***Index Terms*—Eddy currents, electrical machines, excess loss, finite-element analysis, iron loss, magnetic hysteresis, magnetic materials, multilevel converter, pulse width modulation.**

I. Introduction

MULTILEVEL voltage-source inverters are becoming increasingly more popular in electrical machine applications. They are suitable for replacing traditional two-level converters particularly in medium-voltage high-power machines, since the higher number of voltage levels allows using medium-power semiconductors instead of high-power ones [1]. Very recently, different multilevel inverter topologies [2]–[4] as well as control algorithms and modulation techniques [4]–[7] have been under active research. The applications have included converter interfaces to both grid [8], [9] and electrical machines [2], [10], [11].

From the point of view of an electrical machine, the most important property of a multilevel inverter is its ability to produce terminal voltages with lower harmonic contents. This leads to more sinusoidal flux linkages and consequently to better efficiency and smoother torque. However, it seems that the studies on multilevel inverter supplied machines have so far mostly focused on the torque ripple [10], [11], and the power losses have received only a little attention.

Indeed, compared to the huge amount of experimental and theoretical power-loss studies in electrical machines supplied from traditional two-level inverters [12], it is surprising that only [13]–[15] were found to really investigate the effects of multilevel inverters on losses in magnetic cores. In [13], the harmonic losses in a cascaded H-bridge inverter supplied 3-hp (2.2-kW) induction machine were studied. A simple experimental formula for the harmonic losses was compared to no-load measurement results with both two- and seven-level pulse-width modulated (PWM) voltage waveforms. In [14], the optimal control of a three-level T-type converter supplied 7.5-kW induction motor drive was studied. The loss minimizing rotor-flux reference was calculated using a nonlinear equivalent circuit model and experimental data for the harmonic losses at different switching frequencies. In [15], the iron losses in a ring-core setup were studied with multilevel PWM supply-voltage waveforms. In each study [13]–[15], the core losses were found to be significantly reduced when more voltage levels were used.

In this paper, we perform a comprehensive investigation on the effects of multilevel PWM inverters on the losses in magnetic cores. Contrary to the earlier modeling attempts, we apply an accurate dynamic numerical model to account for the iron losses in the core laminations. To compare to the measurements of [15], numerical simulations are first performed for the ring-core inductor with two-, three-, and five-level PWM inverter supplies. It is shown that both the iron losses and their dependence on the switching frequency are significantly reduced with increasing number of voltage levels. Finally, to validate the observations of [13]–[15] in a higher-power range, 150-kVA and 12.5-MW wound-field synchronous machines (see Table I and Fig. 1) are simulated with the finite-element (FE) method with two-, three-, and five-level inverter supplies and relatively low switching frequencies. The predicted core losses of the 150-kVA machine are compared to calorimetric measurements with a two-level inverter supply. Very similarly to the ring-core, the total core losses of the machines decrease when the number of voltage levels is increased.

Combining the physical iron-loss model and FE analysis allows segregation of the losses into different components and thus comprehensive investigation of the loss mechanisms with multilevel inverter supply. By simulating both the 150-kVA and 12.5-MW machines, it is shown that the effect of the supply

Manuscript received July 8, 2014; revised October 3, 2014; accepted November 14, 2014. The work of P. Rasilo was supported by the Finnish Foundation for Technology Promotion. The work of A. Abdallh was supported by the Special Research Fund (BOF) of Ghent University. Paper no. TEC-00489-2014.

P. Rasilo is with the Department of Electrical Engineering and Automation, Aalto University School of Electrical Engineering, FI-00076 Espoo, Finland (e-mail: paavo.rasilo@aalto.fi).

A. Salem, F. De Belie, L. Dupré, and J. A. Melkebeek are with Ghent University, BE-9000 Ghent, Belgium (e-mail: SalemMohamed.Aboubakr Salem@UGent.be; Frederik.DeBelie@UGent.be; luc.dupre@ugent.be; jan.melkebeek@ugent.be).

A. Abdallh is with Ghent University, BE-9000 Ghent, Belgium; and also with the Electrical Power and Machines Department, Cairo University, EG-12613 Giza, Egypt (e-mail: ahmed.abdallh@ieee.org).

Color versions of one or more of the figures in this paper are available online at http://ieeexplore.ieee.org.

Digital Object Identifier 10.1109/TEC.2014.2372095

TABLE I
DATA AND DIMENSIONS OF THE STUDIED MACHINES

Data	Machine I	Machine II
Machine type	generator	motor
Power	150 kVA	12.5 MW
Voltage	400 V	3150 V
Current	217 A	2291 A
Displacement factor	0.8 cap	1
Frequency	50 Hz	50 Hz
Number of pole pairs	2	3
Stator outer diameter	430 mm	1820 mm
Stator inner diameter	300 mm	1340 mm
Air gap	1.2 mm	15 mm
Number of stator slots	48	90

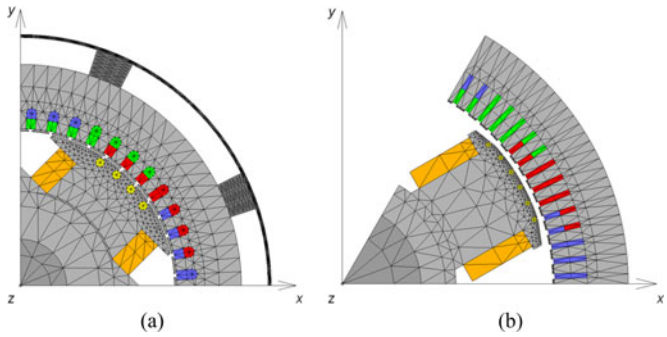

Fig. 1. FE meshes of (a) the 150-kVA machine and (b) the 12.5-MW machine. The two meshes are in different scales.

voltage on the terminal current waveform and loss distribution can vary significantly from one machine to another.

II. MEASUREMENTS

A. Multilevel Inverter Supplied Ring Core

To study the effect of multilevel PWM supply directly on the core material, a standard ring-core setup was used. The core is stacked of 20 0.5-mm-thick rings cut with electrical discharge machining from nonoriented M530/50A electrical steel. The inner and outer radii of the rings are 45 and 55 mm, respectively. The core is equipped with both primary and secondary windings for magnetic-field and flux-density measurements according to IEEE Standard 393-1991 [16].

The iron-loss measurements of the core were first carried out with sinusoidal flux densities of different amplitudes, which were generated by iteratively controlling the supply voltage waveform using a field programmable gate array (FPGA) controller and a power amplifier. In addition, the iron losses were measured under the PWM supply voltage generated by the three different converter topologies shown in Fig. 2. The converters were controlled by means of a carrier-based pulse-width modulation (CBPWM) with a constant modulation index and variable dc-link voltage. The CBPWM technique was implemented on an FPGA digital controller. The PWM was implemented by comparing the carrier sawtooth waveform to a desired target voltage waveform. The target was initially set to the voltage waveform needed to produce the sinusoidal flux density. A similar iterative procedure was then performed until the desired fundamental flux density was reached with an accuracy of 0.1%. Three carrier (switching) frequencies were used at 1.05, 2.55, and 4.95 kHz. More details on the converters and the measurement setup are given in [17] and [15], respectively.

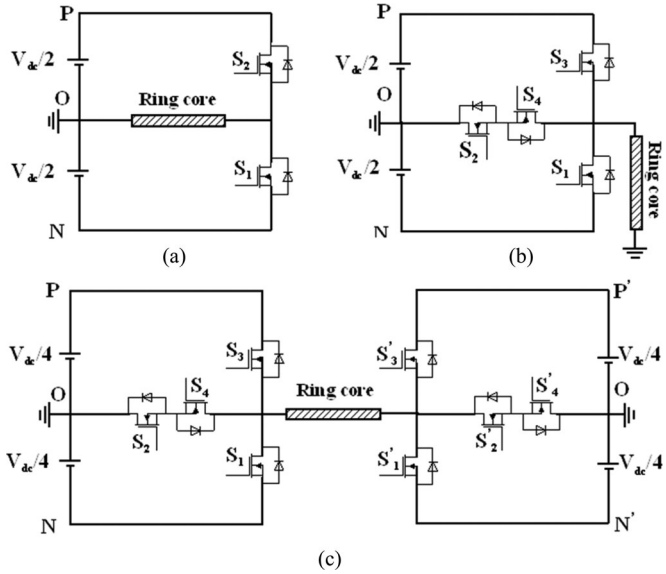

Fig. 2. Single phase circuit of (a) the two-level converter, (b) the T-type three-level converter, and (c) the dual-T-type five-level converter supplying the ring core.

B. Calorimetric Measurements for Synchronous Machine

The 150-kVA machine was used as a test machine for experimental determination of the losses. The stator of the machine is stacked of M600/50A electrical steel sheets while the rotor is stacked of 1-mm steel plates.

The core losses of the machine were experimentally determined using an air-cooled calorimetric setup [18]. The test machine was placed into an insulated polystyrene box, whose coolant air flow was controlled with an exhaust fan. The average air temperatures T and absolute humidity x were measured in both the inlets (subscript in) and outlets (out) using grids of Pt-100 sensors and humidity transducers, which allowed calculation of the heat capacity and the enthalpy increase $\Delta h(T_{\rm in}, T_{\rm out}, x)$ of the air through the calorimeter. The mass flow rate $q_{\rm m}$ was determined by a calibrated orifice plate measurement. The measured quantities allow determining the total heat transferred by the coolant air as

$$\Delta Q = q_{\rm m} \Delta h. \tag{1}$$

To eliminate the heat leakage and the friction and windage losses, the setup was calibrated with dc heater resistors while rotating the test machine without excitation. Direct determination of the total electromagnetic losses of the loaded machine was thus possible by comparison of the heat transferred by the coolant air to the calibration curve.

The core losses were segregated from the total electromagnetic losses by subtracting the dc resistive losses of the stator and field windings. The total core losses of the machine thus

include the iron losses, damper-winding losses, the losses in the frame, shaft and other conducting parts as well as the losses caused by eddy currents and circulating currents in the stator and field windings. The measurements were done with both sinusoidal supply and two-level PWM inverter supply with 1- and 6-kHz switching frequencies and are used here as a reference for the simulations.

III. Methods of Modeling

A. Iron-Loss Model

The iron losses are modeled with the meshless approach comprehensively described in [19]. If an infinitely large core lamination is assumed to lie parallel to the *xy*-plane, the behavior of the magnetodynamic field in the thickness $z \in [-d/2, d/2]$ is described by

$$\frac{\partial^2 \boldsymbol{h}\,(z,t)}{\partial\, z^2} = \sigma \frac{\partial \boldsymbol{b}\,(z,t)}{\partial t} \tag{2}$$

in which σ is the electrical conductivity, and the field strength $\boldsymbol{h}$ and flux density $\boldsymbol{b}$ are parallel to the lamination surface. The solution for (2) is sought as a cosine-series expansion for the flux density

$$\boldsymbol{b}(z,t) = \sum_{n=0}^{N_\mathrm{b}-1} \boldsymbol{b}_n(t)\alpha_n(z) \tag{3}$$

with $\alpha_n(z) = \cos(2\pi n z/d)$. We also expand the field strength so that (2) is identically satisfied:

$$\tilde{\boldsymbol{h}}(z,t) = \boldsymbol{h}_\mathrm{s}(t) - \sigma d^2 \sum_{n=0}^{N_\mathrm{b}-1} \frac{d\boldsymbol{b}_n(t)}{dt}\beta_n(z). \tag{4}$$

Here, $\boldsymbol{h}_s(t)$ is the field on the lamination surface and $\beta_n(z)$ are functions defined so that

$$\alpha_n\,(z) = -d^2 \frac{d^2\beta_n\,(z)}{dz^2} \text{ and } \beta_n\left(\pm\frac{d}{2}\right) = 0. \tag{5}$$

Since the finite series $\boldsymbol{b}(z,t)$ and $\tilde{\boldsymbol{h}}\,(z,t)$ cannot exactly satisfy the constitutive material law $\boldsymbol{h}(\boldsymbol{b})$, it is expressed weakly as

$$\frac{1}{d}\int_{-d/2}^{d/2} \left[\tilde{\boldsymbol{h}}\,(z,t) - \boldsymbol{h}\,(\boldsymbol{b}\,(z,t))\right] \alpha_n\,(z)\,dz = 0 \tag{6}$$

for each $n = 0, \ldots, N_b - 1$. This finally results into a system

$$\begin{bmatrix} \boldsymbol{h}_\mathrm{s}\,(t) \\ \boldsymbol{0} \\ \vdots \end{bmatrix} = \frac{1}{d}\int_{-d/2}^{d/2} \boldsymbol{h}\,(\boldsymbol{b}\,(z,t)) \begin{bmatrix} \alpha_0\,(z) \\ \alpha_1\,(z) \\ \vdots \end{bmatrix} dz + \sigma d^2 \mathbf{C}\frac{d}{dt}\begin{bmatrix} \boldsymbol{b}_0\,(t) \\ \boldsymbol{b}_1\,(t) \\ \vdots \end{bmatrix} \tag{7}$$

from which the flux-density distribution (3) and the surface field $\boldsymbol{h}_\mathrm{s}(t)$ can be solved for a known average flux density $\boldsymbol{b}_0(t)$. The elements of matrix $\boldsymbol{C}$ are

$$C_{mn} = \frac{1}{d}\int_{-d/2}^{d/2} \alpha_m(z)\beta_n(z)dz. \tag{8}$$

The notation in (8) is understood so that the column vectors and matrix $\boldsymbol{C}$ are related to the equations of the system, and the *x* and *y* components of the bold vectors are treated separately.

The local $\boldsymbol{h}(\boldsymbol{b}(z,t))$ is hysteretic and also includes a dynamic contribution from the *excess* eddy-current losses. The hysteretic field strength is obtained from an inverse vector Preisach hysteresis model [20], which projects the flux density into N_φ different directions $\boldsymbol{u}_i = [\cos(i\pi/N_\varphi), \sin(i\pi/N_\varphi)]^\mathrm{T}$, applies an inverse scalar Preisach model to these projections, and sums up the outputs. The excess field-strength part depends on the time derivative of the flux density according to [19], [21], [22]

$$\boldsymbol{h}\,(\boldsymbol{b}) = \sum_{i=1}^{N_\varphi} h_\mathrm{hy}\,(\boldsymbol{b}\cdot\boldsymbol{u}_i)\,\boldsymbol{u}_i + c_\mathrm{ex}\left|\frac{\partial \boldsymbol{b}}{\partial t}\right|^{-0.5}\frac{\partial \boldsymbol{b}}{\partial t}. \tag{9}$$

The local hysteresis classical eddy-current and excess loss densities (in W/m^3) are obtained as

$$p_\mathrm{hy}\,(z,t) = \boldsymbol{h}_\mathrm{hy}\cdot\frac{\partial \boldsymbol{b}\,(z,t)}{\partial t} \tag{10a}$$

$$p_\mathrm{cl}\,(z,t) = \sigma d^2 \sum_{m=0}^{N_\mathrm{b}-1}\sum_{n=0}^{N_\mathrm{b}-1} C_{mn}\frac{d\boldsymbol{b}_m\,(t)}{dt}\cdot\frac{d\boldsymbol{b}_n\,(t)}{dt} \tag{10b}$$

$$p_\mathrm{ex}\,(z,t) = c_\mathrm{ex}\left|\frac{\partial \boldsymbol{b}\,(z,t)}{\partial t}\right|^{1.5}. \tag{10c}$$

The average loss densities are obtained by averaging (10) over the lamination thickness.

B. Electrical Machine Model

The synchronous machines are modeled with a 2-D time-stepping FE model using a magnetic vector potential formulation, so that vector potentials $\boldsymbol{A}_n = A_n\boldsymbol{u}_z$ for which $\boldsymbol{B}_n = \nabla_\mathrm{xy}\times\boldsymbol{A}_n$ correspond to the terms in the flux density expansion (3). Capital letters and ∇_xy denote that the quantities depend on the *xy*-coordinates in the cross section of the machine. The iron losses are included in the FE solution by applying Ampere's law to the rows of system (7)

$$\frac{1}{d}\nabla_\mathrm{xy}\times\int_{-d/2}^{d/2}\boldsymbol{H}\,(\boldsymbol{B}\,(x,y,z,t))\begin{bmatrix}\alpha_0\,(z)\\ \alpha_1\,(z)\\ \vdots\end{bmatrix}dz + \sigma d^2\mathbf{C}\frac{d}{dt}\nabla_\mathrm{xy}\times\begin{bmatrix}\boldsymbol{B}_0\,(x,y,t)\\ \boldsymbol{B}_1\,(x,y,t)\\ \vdots\end{bmatrix} = \begin{bmatrix}\boldsymbol{0}\\ \boldsymbol{0}\\ \vdots\end{bmatrix}. \tag{11}$$

The FE equations are solved together with circuit equations of the windings to allow simulation of the machine with voltage supply. In order to have a good convergence in the FE solution, only single-valued material characteristics are used during the

computation and the hysteresis losses are calculated in the post-processing stage, as justified in [23]. An initial state is calculated with a static FE model and three supply periods are simulated in order to reach a steady state. The iron losses are calculated by integrating (10) over the laminated regions.

C. Multilevel Inverter Model

The inverter voltage waveforms for the FE simulations of the synchronous machines are theoretically generated using the space-vector pulse-width modulation (SVPWM) technique. The SVPWM is a well-performing modulation technique for the control of the different converter topologies, since it produces very small harmonic contents to the output voltage. A complete analysis for SVPWM for two-level and multilevel converters is discussed in detail in [23]–[26]. The theory of operations and circuit diagram of T-type and dual T-type three-phase multilevel converter topologies are discussed in detail in [17].

The terminal voltages for the 150-kVA machine with 400-V fundamental components were produced with both 1- and 6-kHz switching frequencies, which were also used in the calorimetric measurements with the two-level inverter. The 3150-V terminal voltages for the 12.5-MW machine were produced with both 250-Hz and 450-Hz switching frequencies, which are more realistic for this power range.

IV. Results

A. Fitting of Loss-Model Parameters

The ring core was first modeled by solving (7) in a unidirectional configuration, assuming that $\boldsymbol{b}(z,t) = [b(z,t)\,0]^{\mathrm{T}}$, with $b(z,t)$ being the circumferential flux density which varies in the lamination thickness z. The scalar Everett function [20] required for the Preisach model was first determined from low-frequency measurements following the approach of [27]. The lamination conductivity σ and the excess-loss coefficient c_{ex} were then determined by fitting the iron-loss simulations to ring-core measurements with a sinusoidal supply. The obtained values were $\sigma = 2.96\,\mathrm{MS/m}$ and $c_{\mathrm{ex}} = 0.617\,\mathrm{W/m^3(s/T)^{3/2}}$. The losses with these parameters and with different frequencies f and flux-density amplitudes $b_{\max}$ are compared to the measurements in Fig. 3.

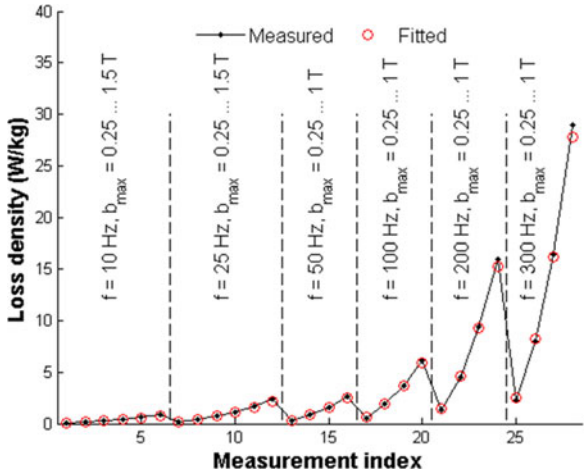

Fig. 3. Fitting of the conductivity and excess-loss coefficient.

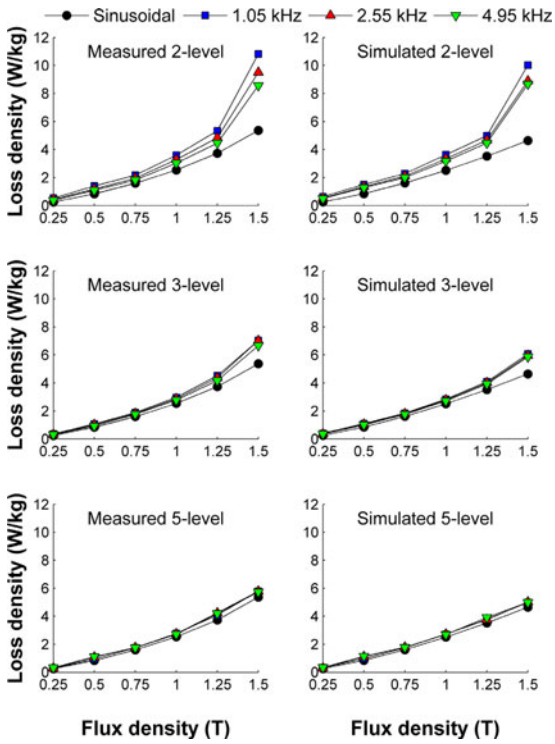

Fig. 4. Measured and simulated loss densities in the ring core with different supply types and fundamental flux-density amplitudes.

B. Ring-Core Losses With Different Inverter Types

After fitting the loss-model parameters, we studied by measurements and simulations how the ring-core losses behave with different supply-voltage waveforms. The iron-loss model was supplied with the measured spatial average flux-density waveforms $b_0(t)$. Fig. 4 shows the measurement and simulation results with two-, three-, and five-level inverters and with 1.05-, 2.55-, and 4.95-kHz switching frequencies and a fundamental frequency of 50 Hz. It is seen that when the number of voltage levels is increased, the losses decrease and approach the values obtained with sinusoidal flux densities. In addition, notable is that the influence of the switching frequency on the losses decreases with increasing number of voltage levels. A very similar behavior is observed in the simulations.

A more careful comparison of the results at fundamental flux densities of 1 and 1.5 T, as well as segregation of the simulated losses into different components, is found in Table II. At 1 T, the simulation results are within 4.6% of the measured losses, while at 1.5 T, the largest error is 15.2%. In most cases, the hysteresis losses comprise a major part of the total losses, while the contribution of the excess losses remains small. When the number of voltage levels is increased, the dynamic loss components are subject to the biggest decreases. Thus, the proportion of the hysteresis loss on the total loss increases with smoother flux-density waveforms. In general, the hysteresis losses seem to

TABLE II
MEASURED AND SIMULATED LOSSES IN THE RING CORE WITH DIFFERENT PWM VOLTAGE WAVEFORMS

Fundamental flux density 1.0 T						
Number of levels	Switching frequency (kHz)	Measured total (W/kg)	Simulated total (W/kg)	Simulated hysteresis (W/kg)	Simulated classical (W/kg)	Simulated excess (W/kg)
2	1.05	3.60	3.63	2.23	0.88	0.52
	2.55	3.28	3.34	1.97	0.84	0.53
	4.95	3.03	3.17	1.85	0.78	0.53
3	1.05	2.97	2.84	1.96	0.55	0.34
	2.55	2.87	2.78	1.91	0.52	0.34
	4.95	2.78	2.71	1.87	0.51	0.33
5	1.05	2.77	2.71	1.94	0.47	0.30
	2.55	2.74	2.72	1.95	0.48	0.30
	4.95	2.71	2.69	1.93	0.47	0.29
Sinusoidal		2.54	2.51	1.86	0.39	0.26
Fundamental flux density 1.5 T						
Number of levels	Switching frequency (kHz)	Measured total (W/kg)	Simulated total (W/kg)	Simulated hysteresis (W/kg)	Simulated classical (W/kg)	Simulated excess (W/kg)
2	1.05	10.8	10.0	4.40	4.00	1.63
	2.55	9.51	8.91	3.53	3.75	1.63
	4.95	8.57	8.68	3.24	3.71	1.72
3	1.05	7.03	6.08	3.26	2.01	0.81
	2.55	7.02	5.95	3.19	1.93	0.83
	4.95	6.67	5.86	3.20	1.82	0.83
5	1.05	5.79	4.99	3.24	1.18	0.56
	2.55	5.79	5.02	3.25	1.19	0.58
	4.95	5.74	5.00	3.26	1.16	0.58
Sinusoidal		5.36	4.64	3.25	0.91	0.47

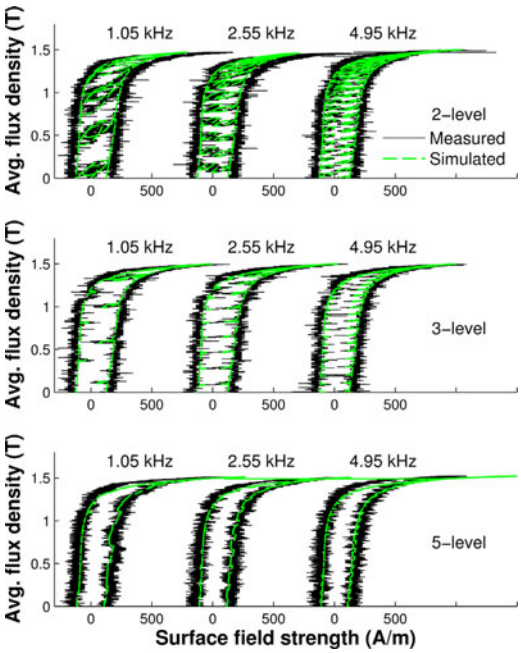

Fig. 5. Measured and simulated dynamic hysteresis loops for the ring core with different types of inverter supply. Color version available online.

be more dependent on the switching frequency than the number of voltage levels.

Fig. 5 shows the $b_0 - h_s$ loops for the different supply waveforms. It is clear that the effect of minor loops reduces as the voltage waveform improves. At the five-level supply, the small effect of the switching frequency on the loop shape is clearly visible.

C. Core Losses in the 150-kVA Machine

The 150-kVA test machine was simulated using the FE method with sinusoidal supply voltage as well as with two-, three-, and five-level inverter voltages generated with the SVPWM technique. Fig. 6 shows the terminal voltage waveforms obtained from the SVPWM for the 1-kHz case. Also the terminal current waveforms and the total harmonic distortions (THD) in the current are shown. The harmonic content reduces from 14.2% to 10.2% when changing from the two-level to the five-level inverter.

Fig. 7 shows the simulated core losses for the different cases and compares these to the calorimetric measurements with the two-level inverter. Very similarly to the ring core, the total core losses decrease significantly as the number of voltage levels is increased. The effect of the switching frequency on the losses is clear in the two-level case, but again becomes negligible with more voltage levels. In this case, however, the difference between the three- and five-level inverters is smaller than in the case of the ring core.

Comparison to the calorimetric measurements shows that the losses simulated at the two-level inverter supply are approximately in the correct ranges. At 25% load, the measured losses are 12–17% higher than the simulated ones while at the rated load, the difference is 23–27%. These differences are most likely caused by the facts that the machine has a skewed stator and conducting end-plates which are not taken into account in the model.

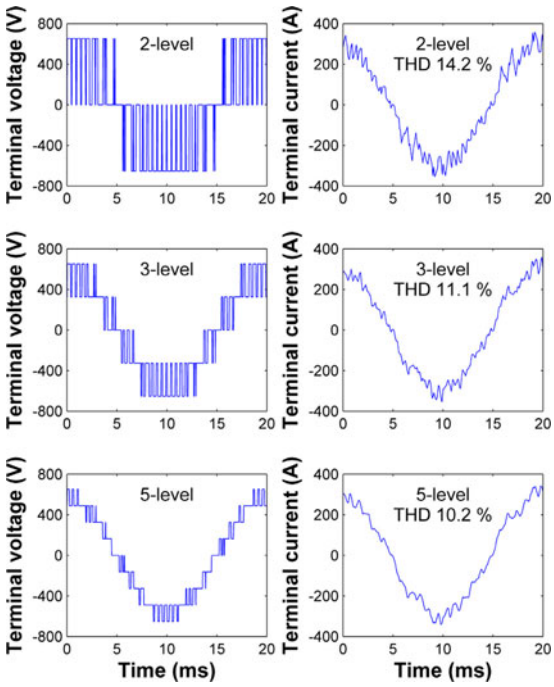

Fig. 6. Simulated terminal voltages, rated-load currents, and current distortions (THD) for the 150-kVA machine at 1-kHz switching frequency.

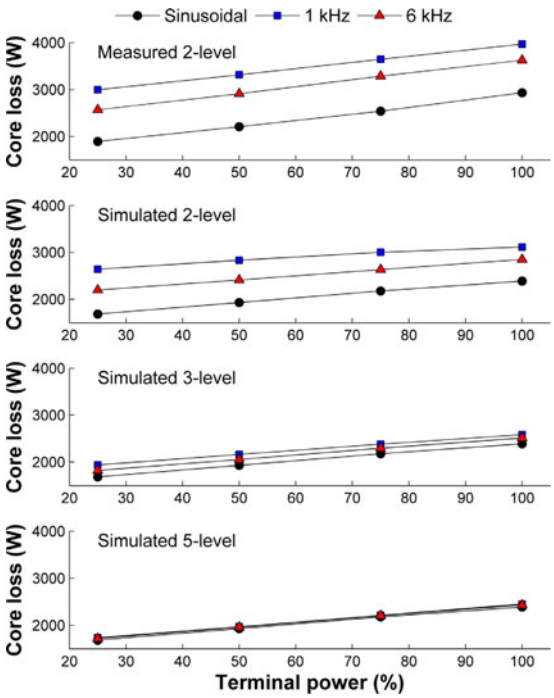

Fig. 7. Core losses in the 150-kVA synchronous machine with different switching frequencies and different numbers of PWM voltage levels.

In addition, the 1-mm rotor laminations have been punched which can significantly increase the losses on the rotor surface due to the deteriorated magnetization properties and contacts between adjacent laminations. A more detailed comparison of the simulations and measurements with different rotor materials

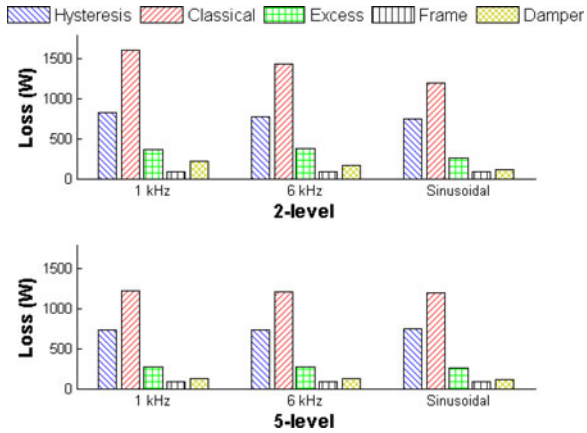

Fig. 8. Segregation of the simulated rated-load core losses of the 150-kVA machine at two- and five-level inverter supplies and comparison to the losses at sinusoidal supply.

is found in [27], while the effect of the punching on the core losses is estimated in [28]. Despite the differences, the effect of the switching frequency on the core losses is realistically predicted by the simulations.

Fig. 8 segregates the simulated rated-load core losses into different components. When the supply is changed from the two-level to the five-level at 1-kHz switching frequency, the hysteresis, classical eddy-current, excess and damper-winding losses, respectively, decrease by 89, 386, 100, and 88 W, or 11%, 24%, 27%, and 40%. The effect on the eddy-current losses in the frame is negligible. Although the excess and damper losses are more sensitive to the voltage waveform than the classical eddy-current losses, the absolute decrease in the classical losses is clearly dominant. The classical eddy-current loss is the greatest loss component in each case due to the high-frequency eddy-current losses induced into the thick rotor laminations. On the other hand, due to the small air gap, the damper winding losses and the current harmonics are dominated by the slot ripple and less affected by the inverter.

D. Core Losses in the 12.5-MW Machine

Fig. 9 shows the terminal voltages and currents for the 12.5-MW machine with 250-Hz switching frequency. In this case, the decrease of the current THD with increasing numbers of voltage levels is significantly larger than in the smaller machine. With larger air gap, the inverter supply dominates over the slot harmonics and thus improving the voltage waveform efficiently reduces the harmonic contents in the current.

The total core losses in Fig. 10 behave very similarly to the smaller machine. However, due to the lower switching frequencies, the differences from the sinusoidal supply at the five-level supply remain larger than in the 150-kVA machine.

As expected from the current THD study, the damper-winding losses are the most affected loss component when the voltage waveform changes. Indeed, when the supply is changed from the two-level to five-level at 250-Hz switching frequency, Fig. 11 shows 3.2, 10.5, 2.1, and 36.8 kW, or 13%, 42%, 27%, and 88%

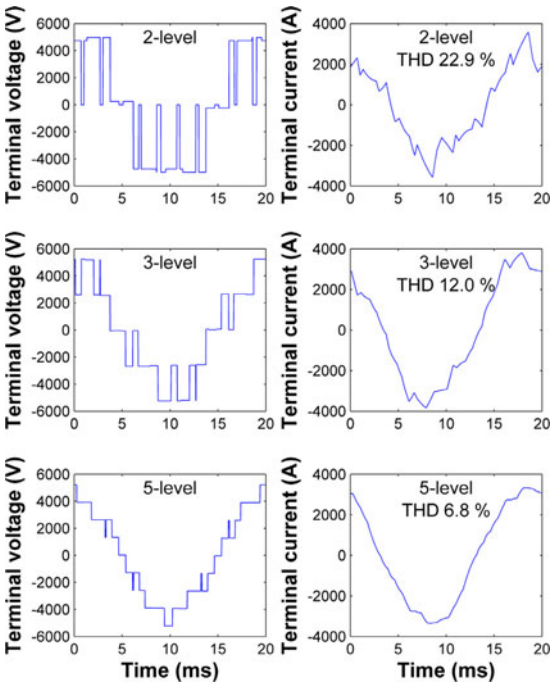

Fig. 9. Simulated terminal voltages, rated-load currents, and current distortions (THD) for the 12.5-MW machine at 250-Hz switching frequency.

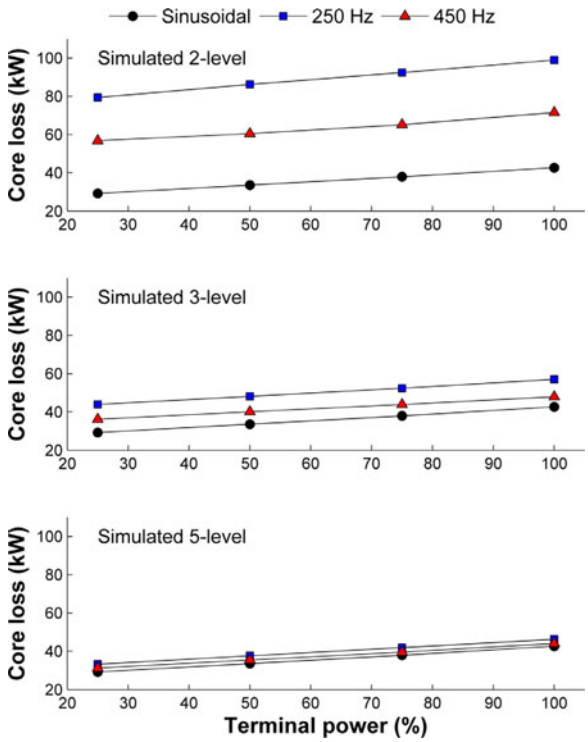

Fig. 10. Simulated core losses in the 12.5-MW machine with different switching frequencies and different numbers of PWM voltage levels.

decreases in the hysteresis, classical eddy-current, excess and damper-winding losses, respectively. The effect on the losses is thus dependent on the construction of the machine.

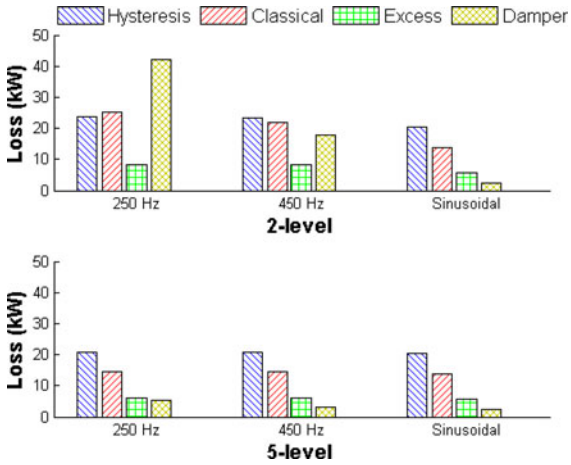

Fig. 11. Segregation of the simulated rated-load core losses of the 12.5-MW machine at two- and five-level inverter supplies and comparison to the losses at sinusoidal supply.

V. Conclusion

The effect of multilevel inverter supply on the power losses in magnetic cores and electrical machines was studied by numerical simulations and experiments. The core losses were found to reduce significantly when more voltage levels were used in the inverter. In addition, it was shown that the effect of switching frequency on the core losses becomes insignificant when more than two voltage levels are used. This is important, since using a lower switching frequency allows reduction of the inverter losses and thus leads to a better total efficiency of the drive.

In the 150-kVA test machine, the largest absolute decrease was observed in the rotor classical eddy-currents losses, while the damper-winding loss decrease dominated in the 12.5-MW machine. In general, the dominant loss components depend on the dimensions and ratings of the machine. In larger machines with larger air gaps, the rotor losses are typically smaller and the proportion of the stator hysteresis losses on the total losses is greater [23]. However, as seen in the case of the 12.5-MW machine, especially the damper winding losses can be very sensitive to the voltage waveform.

As a conclusion, coupling electrical machines to multilevel inverters offers a good means for drive systems to meet better the constantly tightening efficiency requirements. Especially in large machines, huge absolute energy savings are possible. Loss minimization and optimization for a complete drive system offers interesting possibilities for further research.

References

[1] L. G. Franquelo, J. Rodriguez, J. I. Leon, S. Kouro, R. Portillo, and M. A. M. Prats, "The age of multilevel converters arrives," *IEEE Ind. Electron. Mag.*, vol. 2, no. 2, pp. 28–39, Jun. 2008.

[2] K. Mathew, K. Gopakumar, J. Mathew, N. A. Azeez, A. Dey, and L. Umanand, "Medium voltage drive for induction motors using multilevel octadecagonal voltage space vectors," *IEEE Trans. Power Electron.*, vol. 28, no. 7, pp. 3573–3580, Jul. 2013.

[3] A. Masaoud, H. W. Ping, S. Mekhilef, and A. Taallah, "New three-phase multilevel inverter with reduced number of power electronic components," *IEEE Trans. Power Electron.*, vol. 29, no. 11, pp. 6018–6029, Nov. 2014.

[4] Y. Sun, W. Xiong, M. Su, X. Li, H. Dan, and J. Yang, "Topology and modulation for a new multi-level diode-clamped matrix converter," *IEEE Trans. Power Electron.*, vol. 29, no. 12, pp. 6352–6360, Dec. 2014.
[5] E. Levi, I. N. W. Satiawan, N. Bodo, and M. Jones, "A space-vector modulation scheme for multilevel open-end winding five-phase drives," *IEEE Trans. Energy Convers.*, vol. 27, no. 1, pp. 1–10, Mar. 2012.
[6] J. Amini, "An effortless generalized space vector based modulation for N-level flying capacitor multilevel inverter with capacitor voltage balancing capability," *IEEE Trans. Power Electron.*, vol. 29, no. 11, pp. 6188–6195, Nov. 2014.
[7] Y. Deng, K. H. Teo, C. Duan, T. G. Habetler, and R. G. Harley, "A fast and generalized space vector modulation scheme for multilevel inverters," *IEEE Trans. Power Electron.*, vol. 29, no. 10, pp. 5204–5217, Oct. 2014.
[8] M. Hamzeh, A. Ghazanfari, H. Mokhtari, and H. Karimi, "Integrating hybrid power source into an islanded MV microgrid using CHB multilevel inverter under unbalanced and nonlinear load conditions," *IEEE Trans. Energy Convers.*, vol. 28, no. 3, pp. 643–651, Sep. 2013.
[9] P. Samuel, R. Gupta, and D. Chandra, "Grid interface of wind power with large split-winding alternator using cascaded multilevel inverter," *IEEE Trans. Energy Convers.*, vol. 26, no. 11, pp. 299–309, Mar. 2011.
[10] F. Khoucha, M. S. Lagoun, A. Kheloui, and M. E. H. Benbouzid, "A comparison of symmetrical and asymmetrical three-phase h-bridge multilevel inverter for DTC induction motor drives," *IEEE Trans. Energy Convers.*, vol. 26, no. 1, pp. 64–72, Mar. 2011.
[11] U. K. V. Patil, H. M. Suryawanshi, and M. M. Renge, "Closed-loop hybrid direct torque control for medium voltage induction motor drive for performance improvement," *IET Power Electron.*, vol. 7, no. 1, pp. 31–40, Jan. 2014.
[12] A. Boglietti and A. Cavagnino, "Iron loss prediction with PWM supply: An overview of proposed methods from an engineering application point of view," *Elect. Power Syst. Res.*, vol. 80, no. 9, pp. 1121–1127, Mar. 2010.
[13] P. Hothongkam and V. Kinnares, "Investigation into harmonic losses in a PWM multilevel cascaded H-bridge inverter fed induction motor," in *Proc. 7th Int. Conf. Power Electron. Drive Syst.*, Bangkok, Thailand, Nov. 2007, pp. 1043–1048.
[14] M. Schweizer, J. W. Kolar, "High efficiency drive system with 3-level T-type inverter," in *Proc. 14th Eur. Conf. Power Electron. Appl.*, Birmingham, U.K., Aug.-Sep. 2011, pp. 1–10.
[15] A. Salem, A. Abdallh, F. De Belie, L. Dupré, and J. Melkebeek, "A comparative analysis of the effect of different converter topologies on the iron loss of nonoriented electrical steel," *IEEE Trans. Magn.*, to be published.
[16] *IEEE Standard for Test Procedures for Magnetic Cores*, IEEE Standard 393-1991, 1992.
[17] A. Salem, F. De Belie, A. Darba, M. Eissa, S. A. Wasfy, and J. Melkebeek, "Evaluation of a dual-T-type converter supplying an open-end winding induction machine," in *Proc. 39th Annu. Conf. IEEE Ind. Electron. Soc.*, Vienna, Austria, Nov. 10–13, 2013, pp. 749–754.
[18] P. Rasilo, J. Ekström, A. Haavisto, A. Belahcen, and A. Arkkio, "Calorimetric system for measurement of synchronous machine losses," *IET Elect. Power Appl.*, vol. 6, no. 5, pp. 268–294, May 2012.
[19] P. Rasilo, E. Dlala, K. Fonteyn, J. Pippuri, A. Belahcen, and A. Arkkio, "Model of laminated ferromagnetic cores for loss prediction in electrical machines," *IET Electron. Power Appl.*, vol. 5, no. 5, pp. 580–588, Aug. 2011.
[20] I. Mayergoyz, "Vector Preisach hysteresis models (invited)," *J. Appl. Phys.*, vol. 63, no. 8, pp. 2995–3000, Apr. 1988.
[21] G. Bertotti, "General properties of power losses in soft ferromagnetic materials," *IEEE Trans. Magn.*, vol. 24, no. 1, pp. 621–630, Jan. 1988.
[22] L. A. Righi, N. Sadowski, R. Carlson, J. P. A. Bastos, and N. J. Batistiela, "A new approach for iron losses calculation in voltage fed time stepping simulations," *IEEE Trans. Magn.*, vol. 37, no. 5, pp. 3353–3356, Sep. 2001.
[23] P. Rasilo, A. Belahcen, and A. Arkkio, "Importance of iron-loss modeling in simulation of wound-field synchronous machines," *IEEE Trans. Magn.*, vol. 48, no. 9, pp. 2495–2504, Sep. 2012.
[24] B. K. Bose, *Modern Power Electronics and AC Drives*, B. Goodwin, Ed. Upper Saddle River, NJ, USA: Prentice Hall , 2002.
[25] D. G. Holmes and T. A. Lipo, *Pulse Width Modulation for Power Converters: Principles and Practice*. Hoboken, NJ, USA: Wiley, 2003.
[26] S. M. Wasfy, G. M. A. Sowilam, and A. Salem, "Open ends induction motor operation based on a dual inverter," in *Proc. 4th Int. Des. Test Workshop*, Riyadh, KSA, Nov. 2009, pp. 1–6.
[27] P. Rasilo, A. Belahcen, and A. Arkkio, "Experimental determination and numerical evaluation of core losses in a 150-kVA wound-field synchronous machine," *IET Electron. Power Appl.*, vol. 7, no. 2, pp. 97–105, Feb. 2013.
[28] P. Rasilo, A. Abdallh, A. Belahcen, A. Arkkio, and L. Dupré, "Identification of synchronous machine magnetization characteristics from calorimetric core-loss and no-load curve measurements," *IEEE Trans. Magn.*, to be published.

Paavo Rasilo was born in Äänekoski, Finland, in 1983. He received the M.Sc. (Tech.) and D.Sc. (Tech.) degrees in electrical engineering from Aalto University, Espoo, Finland, in 2008 and 2012, respectively.

He is currently a Postdoctoral Researcher in the Department of Electrical Engineering and Automation, Aalto University School of Electrical Engineering, Espoo. His research interests include numerical modeling of electrical machines, as well as power losses and magnetomechanical effects in soft magnetic materials.

Aboubakr Salem was born in 1982. He received the B.Sc. and M.Sc. degrees in electrical engineering from Helwan University, Helwan, Egypt, in 2004 and 2009, respectively. He received a scholarship funded by European Communitty Action Scheme for the Mobility of University Students (ERASMUS) modus to continue his Ph.D. study in Ghent University, Ghent, Belgium.

His research interests include power electronic converters design, control, and performance evaluation, especially for multilevel voltage-source converters for ac drives, renewable energy, and smart grid applications.

Ahmed Abdallh was born in 1980. He received the B.Sc. and M.Sc. degrees in electrical engineering from Cairo University, Giza, Egypt, in 2003 and 2006, respectively, and the Ph.D. degree in electromechanical engineering from Ghent University, Ghent, Belgium, in 2012.

Since 2012, he has been a Postdoctoral Researcher for the Bijzonder Onderzoeksfonds (BOF) at Ghent University. His research interests include numerical methods for electromagnetics, especially the magnetic materials identification using inverse problems.

Frederik De Belie was born in Belgium, on October 9, 1979. He received the M.Sc. degree in electromechanical engineering and the Ph.D. degree from Ghent University, Ghent, Belgium, in 2002 and 2010, respectively.

He is currently a Postdoctoral Assistant at the Department of Electrical Energy, Systems, and Automation, Ghent University, performing research mainly on advanced control and identification of modern electrical drives.

Luc Dupré was born in 1966. He received the Graduate degree in electrical and mechanical engineering in 1989 and the Doctorate degree in applied sciences in 1995 from the University of Gent, Ghent, Belgium.

He is currently a Full Professor with the Faculty of Engineering and Architecture, Ghent University. His research interests mainly include numerical methods for electromagnetics, modeling, and characterization of soft magnetic materials, micromagnetism, inverse problems, and optimization in (bio)electromagnetism.

Jan A. Melkebeek (SM'84) was born in Gent, Belgium, on February 20, 1952. He received the "Ingenieur" degree in electrical and mechanical engineering in 1975, the degree of Doctor in applied sciences in 1980, and the degree of "Doctor Habilitus" in electrical and electronic power technology in 1986 from the University of Gent, Gent.

Since 1987, he has been a Professor in Electrical Engineering (electrical drives, electrical machines, and power electronics) with the Engineering Faculty, University of Gent, where he is the Head of the Department of Electrical Power Engineering, Systems, and Automation, and the Director of the Electrical Energy Laboratory. He was a Visiting Professor at the Université Nationale de Rwanda in Butare, Rwanda, Africa, in 1981, and a Visiting Assistant Professor at the University of Wisconsin–Madison, Madison, WI, USA, in 1982. His teaching activities and research interests include electrical machines, power electronics, variable frequency drives, and control systems theory applied to electrical drives.

Prof. Melkebeek is a Member of the Koninklijke Vlaamse Ingenieursvereniging (K.VIV), the Koninklijke Belgische Vereniging van Elektrotechnici (KBVE-SRBE), and a Fellow of the Institution of Engineering and Technology (IET). He served as the President of the IEEE Benelux Industry Applications Society-Power Electronics Society (IAS-PELS) joint chapter from 2002 to 2003, and is a long-time Member of the IEEE-IAS Electric Machines Committee, the IEEE-IAS Electric Drives Committee, and the IEEE-Power and Energy Society Machine Theory Subcommittee.